Available online at www.sciencedirect.com
SCIENCE DIRECT®
Journal of Nuclear Materials 337–339 (2005) 897–901
journal of nuclear materials
www.elsevier.com/locate/jnucmat

Density functional theory and molecular dynamic studies of hydrogen interaction with plasma-facing graphite surfaces and the impact of boron doping

Y. Ferro [a,*], A. Jelea [a,b], F. Marinelli [a], C. Brosset [b], A. Allouche [a,*]

[a] *Physique des Interactions Ioniques et Moléculaires Université de Provence and CNRS, Marseille, France*
[b] *Association Euratom-CEA, CEA/DSM/DRFC, CEA-Cadarache 13108 Saint Paul lez Durance, France*

Abstract

Quantum calculations are performed on hydrogen interaction with pure or doped graphite. Particular attention is given to the influence of boron doping of the (0001) basal plane of graphite on molecular hydrogen recombination. These structural results are also the first step of the series of Quantum Molecular Dynamics calculations which take into account the total system temperature and initial kinetic energy of the hydrogen atoms impinging the substrate. Models are also proposed for saturation coverage of graphite (0001) terrace and (1010) terrace edge.

PACS: 68.43.Bc; 68.43.Vx; 71.15.Pd; 68.43.−f
Keywords: Boronized graphite; Plasma facing components; Molecular dynamics simulations; Graphite materials; Hydrogen retention

1. Introduction

The ITER design currently recommends using carbon fiber composites (CFC) for the divertor's area near the strike-points, at least before the DT (deuterium–tritium) operation [1]. CFC is a low-Z carbon-based material chosen because of its high thermal shock resistance and tolerance to off-normal events. The main drawback of carbon is its strong chemical reactivity to hydrogen isotops atoms (H/D/T), which leads to chemical erosion/redeposition mechanisms in carbon-lined fusion devices. Since tritium retention in carbon co-deposits remains one of the crucial plasma-material interaction (PMI) issues for fusion reactor development [2,3], modeling work is carried out focusing on carbon chemical erosion/redeposition processes [4,5]. Such computer modeling requires reflection probability for atomic and molecular species and energy distribution for reflected molecules. In order to calculate data for low-energy carbon/hydrocarbon reflection, molecular dynamics calculations were performed in order to improve the models [4,6]. Most of these calculations use the empirical many-body Brenner potential [7]. In this paper, we present potential energy surfaces (PES) and molecular dynamic (MD) results based on density functional theory (DFT). These results concern the adsorption, diffusion and recombination of atomic hydrogen on the basal

* Corresponding authors. Address: Campus Universitaire de Saint Jérôme, UMR6633, service 224, 13397 Marseille cedex 20 (Y. Ferro).
E-mail addresses: yves.ferro@up.univ-mrs.fr (Y. Ferro), alain.allouche@up.univ-mrs.fr (A. Allouche).

0022-3115/$ - see front matter
doi:10.1016/j.jnucmat.2004.09.059

terraces and edge of terraces of graphite and on boron-doped graphite. The aim of this work is to investigate hydrogen-carbon-based material interactions which are not based on empirical assumptions. Our general objective is to provide modeling-teams with realistic quantum data to complement and upgrade the existing empirical data in order to further improve PMI modeling work. Readers specifically interested in a comparison between DFT and empirical Brener potentials may have a look on Ref. [8].

DFT study of hydrocarbon adsorption and production from perfect graphite surface has been published elsewhere [9–13]. The reader may find all the computational methods and technical details in these articles.

2. Hydrogen on a pure graphite surface

2.1. Potential energy surfaces

We investigated the electronic interactions between H atoms and periodic graphite surface from potential energy surfaces (PES) issued from DFT calculations (Dmol3 computer code [14]) in order to help understanding the dynamical mechanisms investigated in the following section.

We calculated the PES for an H atom approaching the [0 0 0 1] graphite perpendicularly to the surface, direction *I* in Fig. 1. We determined an activation barrier of adsorption of about $E^{\ddagger} = 20$ kJ mol^{-1}, at 2.0 Å in good agreement with other investigations [15,16]. The minimum energy lies at 1.5 Å from the surface and the energy value at this point is −78 kJ/mol [12]. Hence, the total energy for desorption is 98 kJ mol^{-1}.

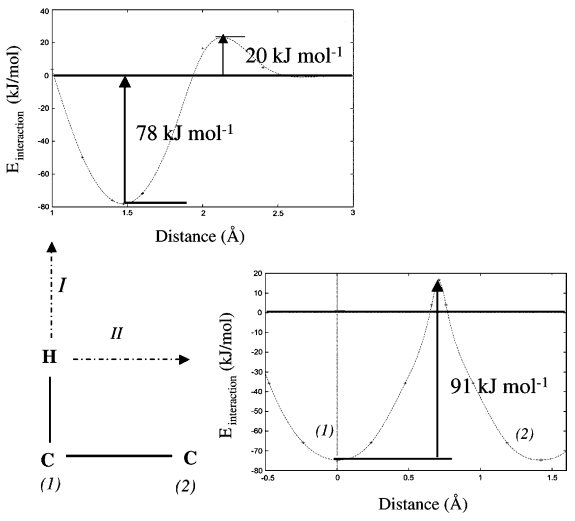

Fig. 1. Potential Energy Surfaces associated to parallel and perpendicular interaction of hydrogen with graphite surface (energy in kJ mol^{-1} vs C–H distance in Å).

The energy of activation for the parallel diffusion (direction *II* in Fig. 1) of adsorbed hydrogen on a graphite layer along a C–C bond is 91 kJ mol^{-1}. At the transition state, with H in the middle of the C–C bond, the total energy of the system is 17 kJ mol^{-1} above that of the reference system, which is the energy of an isolated H atom *plus* that of the graphite layer. However, desorption does not occur; a weak activation energy would be necessary for this [9,16].

From these results, it can be predicted in view of a dynamical study that (i) a kinetic energy of at least 20 kJ mol^{-1} is needed for the adsorption of an H atom on the pure graphite surface and (ii) an adsorbed H atom on a pure graphite surface remains bonded as long as its maximum kinetic energy is below 98 kJ mol^{-1}. Above this value, two processes become possible depending on the vibration direction of H. Perpendicularly to the surface, it is desorption that occurs. In the parallel direction, a competition occurs between the diffusion and desorption processes at the transition state.

2.2. Dynamics of H-graphite interaction on terraces

At the starting point of the simulation (Verlet algorithm, Abinit computer code [17]), the incident atom is located at 2.5 Å from the target C and its trajectory direction forms an angle α ranging from 30° to 150° (using 30° steps) with respect to the surface. The other parameter defining the MD simulation is the incident kinetic energy E_{kin}, which is scanned from 0.2 eV to 0.8 eV by 0.2 eV steps.

The Verlet algorithm is used to resolve the equation of motion by combining the second order Taylor expansion of each particle coordinate $\mathbf{r}$ at $(t + \Delta t)$ and $(t - \Delta t)$. The Verlet algorithm thus deduce

$$\mathbf{r}(t+\Delta t) = 2\mathbf{r}(t) - \mathbf{r}(t-\Delta t) + \mathbf{f}(t)/m.\Delta t^2, \qquad (1)$$

which determines the particle position from the position of the two former steps and the ab-initio calculated $f(t)$ force using Hellman–Feynman theorem.

Incident energies below 0.2 eV (21 kJ/mol) do not yield hydrogen atom adsorption. Incident energies larger than 1 eV (96 kJ/mol) give elastic or quasi-elastic collisions without adsorption. This is in very good agreement with the above assumption made from PES calculations. All the simulations start from the gradient optimized surface.

Direct collisions ($\alpha = 90°$) also do not produce adsorption, whatever the incident energy. An energy transfer from H to the lattice vibration modes does occur but is not sufficient for H to remain bonded to the surface. The scattering process becomes efficient for adsorption when the incident angle is lower than the surface. For $\alpha = 30°$, the scattering process yields adsorp-

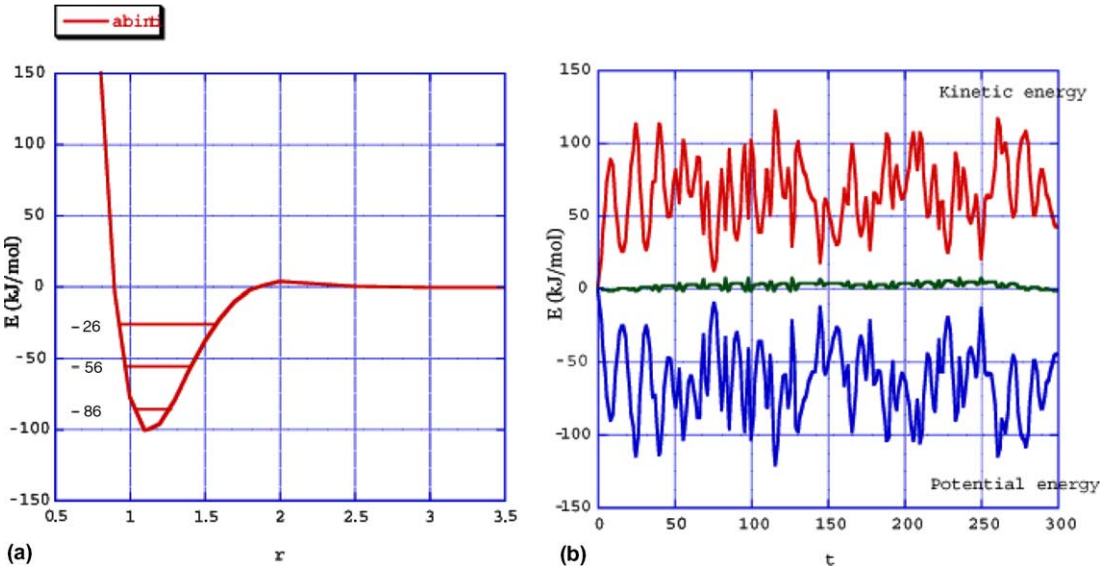

Fig. 2. Verlet simulation of hydrogen atom adsorption on pure (0 0 0 1) graphite surface (energy in kJ mol^{-1}, time in fs and lengths in Å): (a) adsorption energy vs C–H distance (b) kinetic (upper curve), potential (lower curve) and total energy variations vs time simulation.

tion for incident energies ranging from 0.2 to 0.4 eV. For $\alpha = 150°$, this domain extends from 0.4 to 0.6 eV. Fig. 2 presents the case $\alpha = 30°$ and $E_{kin} = 0.2$ eV. The left-side part shows the DFT interaction energy as a function of the C–H distance. Vibration energy levels are calculated within the harmonic approximation from the Morse oscillator fitting the ab initio numerical results. On the right-side part of Fig. 2 are shown the variations of all the energy components over time. During the first few steps, the potential energy increases in absolute value until it reaches the potential energy minimum at -86 kJ mol^{-1}. Then, the CH bond vibrates around its equilibrium position and an exchange of potential and kinetic energies takes place according to the conservation energy principle.

On the whole, we calculated 20 trajectories, each one being 350 fs long. The total number of them yielding adsorption is 6, therefore the sticking probability resulting from these very limited simulations is about 30% using all the incident angles and energies in the domain mentioned above. This sticking coefficient is of the same range of magnitude as the experimental results given by Zecho et al. [18], between 25% and 50% for D and close to 40% for H. It is also similar to the coefficient calculated by Ma et al. [19,20] on carbon single-wall nanotubes, 34.4%.

2.3. Diffusion of H on a graphite layer

It has been shown above that an isolated H atom adsorbed on the pure graphite surface has to overcome a barrier of 91 kJ mol^{-1} to diffuse along the C–C bonds. This PES study is complemented here with Verlet MD simulations where the adsorbed atom experiences an energy impulse parallel to the surface and directed towards the first neighboring carbon atom. The energy impulses E_{kin} ranged from 0.2 to 4 eV. Only for $E_{kin} = 1.2$ eV can H jump from its starting position to the next one. Smaller energies are only converted to vibration–rotation modes while larger energies yield hydrogen desorption.

The energy range for efficient diffusion is very narrow and centered around 1.0 eV, as we predicted above from PES calculations. As a consequence, H diffusion on a graphite layer mainly results from a series of adsorption-desorption processes rather than continuous diffusion along C–C bond on the surface.

3. Modification of the H-graphite interaction by impurities and defects

The doping element investigated here is boron. It is inserted into the graphite lattice by substitution of carbon atoms. The graphitic-doped surfaces (C_3B) we modeled contain 25% of boron at. Discussed here are the changes induced by boron on H adsorption, diffusion and recombination on the surface.

Another defect studied here concerns the terrace borders. The terrace edge can be constituted from zigzag patterns (1 0 1 0 direction) or from boat-shaped edges (1 1 2 1 direction), it has already been shown that the former is more reactive [21] and this is the one chosen in this study.

3.1. Effects of boron impurity

Boron doping dramatically changes the adsorption energy from $-79\ \mathrm{kJ\ mol^{-1}}$ on pure graphite to $-163\ \mathrm{kJ\ mol^{-1}}$ on C_3B. Adsorption always occurs on carbon atoms [11].

These larger binding energies are in good agreement with experimental observations [22] that have shown that the H/C ratio increases from 0.4 to 0.6 from pure graphite to boron-doped graphite. However, while H retention increases, it is also shown that H + H recombination is facilitated since H desorbs at lower temperatures under thermal desorption spectroscopy (TDS) conditions. These observations seem contradictory and have motivated the following study.

We first investigated two modes of H diffusion as a first step yielding recombination: diffusion along a C–C bond or along a C–B bond on the surface. In both cases, $E^{\ddagger}$ is half the activation barrier on pure graphite ($50\ \mathrm{kJ\ mol^{-1}}$ and $54\ \mathrm{kJ\ mol^{-1}}$ respectively instead of $91\ \mathrm{kJ\ mol^{-1}}$) [11]. Moreover, and as a consequence of the larger binding energy induced by boron for H, the energy of the system at the transition state is $113\ \mathrm{kJ\ mol^{-1}}$ below that of the reference system. From the dynamics point of view, this implies that H does not have to desorb in order to diffuse, as opposed to the case of pure graphite.

We calculated the activation energy for the H + H recombination step on pure graphite and boron doped graphite (C_3B). We found activation energies of $272\ \mathrm{kJ\ mol^{-1}}$ [10] and only $9\ \mathrm{kJ\ mol^{-1}}$ [12] respectively. The latter, a very low value, is due to the ability of boron to form bridge bonds that stabilize the transition state.

As a conclusion, on a pure graphite surface and under TDS conditions, H has to desorb in order to recombine. The activation energy for H (free) + H (ads) recombination being zero [9], the energy for H_2 recombination is that for H desorption: $98\ \mathrm{kJ\ mol^{-1}}$.

On the contrary, recombination occurs on the C_3B surface. The rate-limiting step is diffusion, which occurs with an activation energy of 50 to $54\ \mathrm{kJ\ mol^{-1}}$. Hence, the overall activation energy is half reduced. This result is in good agreement with the enhanced ability for H_2 recombination induced by boron under TDS conditions.

Hence, boron increases H retention by inducing a better binding of H to the surface. It also increases recombination by half-reducing the activation energy of reaction that occurs according to a modified mechanism.

3.2. Adsorption on terrace edge

The edge is modeled as shown in Fig. 3(a). The hydrogen atoms are injected into the system one after another in order to mimic a progressive saturating hydrogen coverage. The adsorption energy of the n-th H is calculated from the $(n-1)$-H system through:

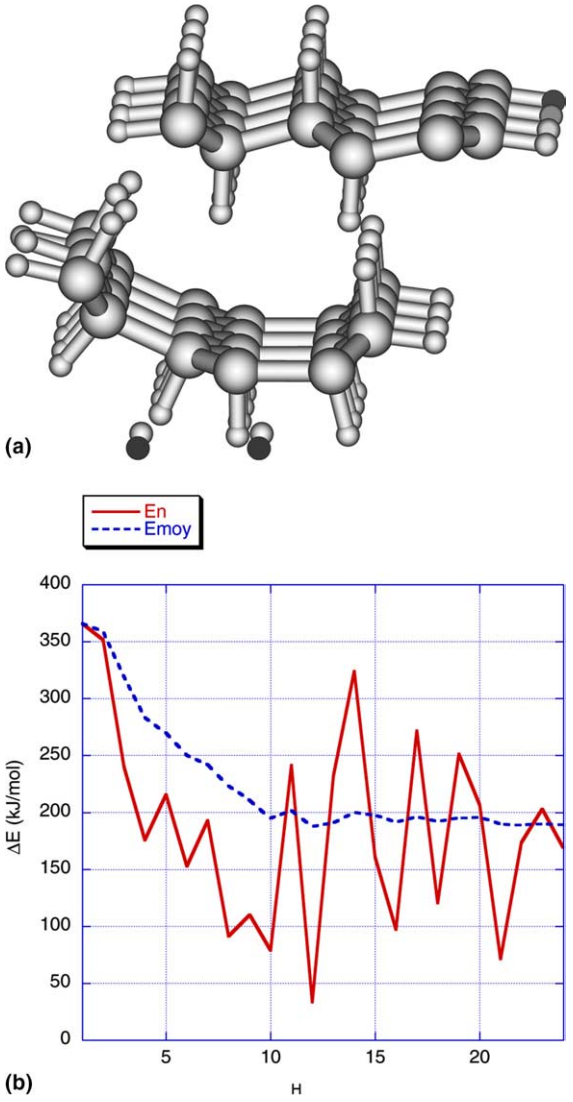

Fig. 3. Hydrogen adsorption on terrace edges: (a) Final structure of the edge of the terrace after H atom saturation. The larger spheres represent C atoms, the smallest ones Hs. (b) Adsorption energy $-E^{n}_{\mathrm{ads}}$ ($\mathrm{kJ\ mol^{-1}}$) of the successive Hs adsorption (solid lines) calculated according to Eq. (2). In abscissa figured the number of adsorbed Hs, in discontinuous line are figured the average adsorption energies $-E^{n}_{\mathrm{av}}$ ($\mathrm{kJ\ mol^{-1}}$) calculated according to Eq. (3).

$$-E^{n}_{\mathrm{ads}} = E^{n} - E^{n-1} - E^{\mathrm{H}}, \tag{2}$$

where E^{n} is the total energy of the system constituted by the pure substrate + n adsorbed Hs and E^{H} is the H atom total energy. The average value of the adsorption energy is calculated as:

$$-E^{n}_{\mathrm{av}} = E^{n} - E^{0} - nE^{\mathrm{H}}, \tag{3}$$

where E^{0} is the energy of the pure graphite surface.

The adsorption energies vs hydrogen coverage are displayed in Fig. 3(b) which also exhibits the average adsorption energy for n H atoms. The first two atoms adsorb on the very edge of the two layers forming strong C–H chemical bonds. After that, the hydrogen atoms preferably saturate the lower layer represented in Fig. 3(a) and always on the same side, consequently giving to the plane an incurving appearance and seemingly forming some kind of tube. In fact, formation of carbon nano-tubes has already been reported in tokamaks [23].

With hydrogen atom #16, the lower carbon layer is saturated and the H atoms begin to adsorbed on the upper one, but the process now occurs in an alternated mode generating armchair-shape patterns. At saturation, the number of hydrogen atoms is 25, thus achieving a coverage rate of 1:1.

The E^n values displayed in Fig. 3(b) exhibit a curious serrated aspect. Except for the first two Hs, the adsorption energy of the odd-numbered Hs is always smaller than the next even-numbered ones as far as the H adsorbs on the bottom layer. At saturation of this layer, the H adsorbed on the top layer and the odd number atoms are more energetically adsorbed than even ones. However, the general physiognomy of the curve is preserved. This reflects the fact that the first H perturbs the surface, changing the hybridization state of the adsorbent carbon which becomes pyramidal. The next H benefits from this perturbation and is more energetically bonded. It is obvious that the successive E_{ads} calculated depend on the adsorption sites. This behavior is not a general law and it is broken for the adsorbed Hs #13,15 and 20. In case of H#13, the gradient minimization imposes migration of an already adsorbed atom from the lower layer to the upper one on an edge C. The adsorption of H#15 occurs after saturation of the lower layer, the adsorption site is an edge C of the upper layer which was singly hydrogenated but its hybridization state was already sp3. Hs # 20 and 22 adsorb on the inner carbon atoms of the upper layer, these carbon was frozen in order to maintain the inter-layer distance.However, and from the reactivity point of view, it may be concluded that:

(i) the edge is very reactive for the first H atoms, (ii) its reactivity remains important after successive adsorption. E_{ads} converges to a value of about -200 kJ mol^{-1}, that is roughly three times greater than on graphite.

4. Conclusion

We have shown the important coherence and complementarities between PES and dynamic calculation to model H graphite interaction. Our results are in good agreement with experiment and provide new insights into the mechanism of retention, diffusion and recombination of H on graphite layers. The impact of impurities and defects has also been investigated. The general effect is to increase graphite reactivity toward H. These effects have been quantified and mechanisms (or the way they are modified) have been proposed.

Acknowledgment

This work is supported by the Euratom-CEA Association in the framework of the LRC (Laboratoire de Recherche Conventionné CEA/DSM – Université de Provence PIIM). All the calculations were performed at IDRIS, the CNRS computing center.

References

[1] G. Federici et al., J. Nucl. Mater. 313 (2003) 11.
[2] R.A. Causey, J. Nucl. Mater. 300 (2002) 91.
[3] M. Mayer et al., J. Nucl. Mater. 290 (2001) 381.
[4] J.N. Brooks et al., J. Nucl. Mater. 313 (2003) 424.
[5] A. Kirschner, V. Philipps, J. Winter, U. Kogler, Nucl. Fus. 40 (5) (2000) 989.
[6] Ph. Chappuis et al., J. Nucl. Mater. 290–293 (2001) 245.
[7] D. Alman, D. Ruzic, J. Nucl. Mater. 313–316 (2003) 182.
[8] N. Marks et al., Phys. Rev. B 65 (2002) 075411.
[9] Y. Ferro, F. Marinelli, A. Allouche, J. Chem. Phys. 116 (2002) 8124.
[10] Y. Ferro, F. Marinelli, A. Allouche, Chem. Phys. Lett. 368 (2003) 609.
[11] Y. Ferro, F. Marinelli, A. Allouche, C. Brosset, J. Chem. Phys. 118 (2003) 5650.
[12] Y. Ferro, F. Marinelli, A. Allouche, A. Jelea, J. Chem. Phys. 120 (2004) 11882.
[13] A. Allouche, Y. Ferro, A. Jelea, F. Marinelli, submitted for publication.
[14] B. Delley, J. Chem. Phys. 92 (1990) 508.
[15] X. Sha, B. Jackson, Surf. Sci. 496 (2002) 318.
[16] L. Jeloaica, V. Sidis, Chem. Phys. Lett. 300 (1999) 157.
[17] X. Gonze et al., Comput. Mater. Sci. 25 (2002) 478.
[18] T. Zecho et al., J. Chem. Phys. 117 (2002) 8486.
[19] Y. Ma et al., Phys. Rev. B 63 (2001) 115422.
[20] Y. Ma et al., Phys. Lett. A 288 (2001) 207.
[21] F.H. Yang, R.T. Yang, Carbon 4 (2002) 437.
[22] A. Schenk et al., J. Nucl. Mater. 220 (1995) 767.
[23] Ph. Chappuis et al., J. Nucl. Mater. 290–293 (2001) 245.